SCIENTIFIC REPORTS
nature research

Check for updates

OPEN

Synthesis of mesoporous SnO_2/NiO nanocomposite using modified sol–gel method and its electrochemical performance as electrode material for supercapacitors

Bhaskar Varshney[1,2], M. J. Siddiqui[1], A. Hakeem Anwer[3], M. Zain Khan[3], Faheem Ahmed[4], Abdullah Aljaafari[4], Hassan H. Hammud[5] & Ameer Azam[2]✉

In this research work, SnO_2, NiO and SnO_2/NiO nanocomposites were synthesized at low temperature by modified sol–gel method using ultrasonication. Prepared samples were investigated for their properties employing various characterization techniques. X-ray diffraction (XRD) patterns confirmed the purity and phase of the samples as no secondary phase was detected. The average crystallite size of the nanocomposites was found to decrease from 19.24 to 4.53 nm with the increase in NiO concentration. It was confirmed from SEM micrographs that the material has mesoporous morphology. This mesoporous morphology resulted in the increase of the surface to mass ratio of the material, which in turn increases the specific capacitance of the material. The UV–Visible spectra showed the variation in the band gap of SnO_2/NiO at different weight ratio ranging from 3.49 to 3.25 eV on increasing NiO concentration in the samples. These composites with different mass ratio of SnO_2 and NiO were also characterized by FT-IR spectroscopy that showed shifting of the peaks centered at 545 cm^{-1} in the spectra for NiO/SnO_2 nanocomposite. The analysis of the electrochemical performance of the material was done with the help of cyclic voltammetry and Galvanostatic charge–discharge. The specific capacitance of the synthesized samples with different concentration of SnO_2 and NiO was analyzed at different scan rates of 5 to 100 mV/s. Interestingly, 7:1 mass ratio of NiO and SnO_2 (SN7) nanocomposite exhibited a maximum specific capacitance of ~ 464 F/g at a scan rate of 5 mV/s and good capacitance retention of 87.24% after 1,000 cycles. These excellent electrochemical properties suggest that the SnO_2/NiO nanocomposite can be used for high energy density supercapacitor electrode material.

As a result of increase in energy consumption demands, conventional energy sources on the earth are getting exhausted day by day. Thus, the whole world has concentrated on energy-related research. The best alternative for the energy is renewable energy. However, the main problem with this type of energy is that it is not available continuously. Hence, it is necessary to store this type of energy when it is available so that it can be utilized whenever needed. Li-ion batteries and supercapacitors are widely used energy storage devices[1–3]. Conventional

[1]Department of Electronics Engineering, Z.H. College of Engineering and Technology, Aligarh Muslim University, Aligarh, Uttar Pradesh 202002, India. [2]Department of Applied Physics, Z.H. College of Engineering and Technology, Aligarh Muslim University, Aligarh, Uttar Pradesh 202002, India. [3]Environmental Research Laboratory, Department of Chemistry, Faculty of Sciences, Aligarh Muslim University, Aligarh, Uttar Pradesh 202002, India. [4]Department of Physics, College of Science, King Faisal University, P.O. Box 400, Al-Ahsa 31982, Saudi Arabia. [5]Department of Chemistry, College of Science, King Faisal University, P.O. Box 400, Al-Ahsa 31982, Saudi Arabia. ✉email: azam2288@gmail.com

capacitors have high power density with low energy density and the batteries have high energy density with low power density. A supercapacitor with its high power and cycling is a device that is bridging the gap between the batteries and the conventional capacitors[4,5]. In recent years, lot of research on the electrode material for the supercapacitor has improved the performance of this device[6]. For the electrode material of supercapacitor many transition metal oxides have taken into account and they exhibit high energy performance which is beneficial for supercapacitors development[7–10]. For supercapacitor electrodes, metal oxides behave as promising materials as they show pseudocapacitive effect. Metal oxides such as NiO[11], SnO_2[12], Fe_3O_4[13–15], Fe_2O_3[16,17], Co_3O_4[18], RuO_2[19–22], MoO_3[23], ZnO[24,25], CuO[26,27] and WO_3[28] have been developed as promising candidates for supercapacitor electrodes. From these metal oxides, SnO_2 is a low cost, non-toxic and easily synthesizable nanomaterial[29]. Simple effective sol–gel method for the synthesis of SnO_2 nanoparticles has been reported by Aziz et al.[30]. SnO_2 has been used in various applications like photocatalysis, gas sensors and Li-ion batteries[31,32]. SnO_2 are widely used group among the important oxides that has been used for electrode of supercapacitors[11,33,34]. As NiO can exhibit multiple oxidation states, it favors the condition of fast redox reaction that in turn leads to high specific capacitance[35] and its composites are widely used in electrochemical applications [36–40]. Composites made by mixing different metal oxides exhibit very huge electrochemical capacitance[41]. Porous materials are the promising materials for the electrodes of supercapacitor as they provide more active surface for electron transfer and mass transport that in turn results in high specific capacitance.

In the present study nanocomposites of NiO and SnO_2 were synthesized with different mass ratio by using a modified sol–gel route and their electrochemical properties for the electrode materials for supercapacitors have been investigated. In the modified of sol–gel route, ultrasonication was used for mixing the samples at low temperature leading to a mesoporous structure of the composite material.

Experimental details

Materials used. All chemicals were used without further purification. Sodium dodecyl sulphate (SDS) (90%) was purchased from CDH, stannous chloride dihydrate (98%), nickel chloride hexahydrate (97%), ethylene glycol (99%), isopropyl alcohol (99%) and sodium hydroxide (97%) were obtained from Fisher Scientific and methanol (99%) was purchased from S. D. Fine Chemicals.

Synthesis of SnO_2 nanoparticles. Firstly, 10 ml distilled water, 5 ml ethylene glycol and 5 ml ethanol were mixed and 1 M SDS was dissolved in the solution. Then 0.1 M stannous chloride dihydrate ($SnCl_2{\cdot}2H_2O$) was added slowly to the prepared solution and mixed with the help of sonicator in ice bath to maintain low temperature. NaOH solution of 10 M concentration was prepared and then added to the above solution drop wise until the pH becomes 10. Consequently, washing of the sample was done several times by centrifuge. Methanol and distilled water were used for removing Cl^- ions and excess NaOH and SDS. The sample was dried using vacuum oven at 100 °C for 24 h and calcined in a furnace at 400 °C for 3 h. Finally, the sample was grinded using agate mortar to get the SnO_2 nanoparticles.

Synthesis of NiO nanoparticles. Firstly, 50 ml isopropyl alcohol and 50 ml distilled water were mixed and 0.25 M SDS was dissolved in the solution. Then 0.1 M nickel chloride hexahydrate ($NiCl_2{\cdot}6H_2O$) was added to the prepared solution and mixed with the help of sonicator in ice bath to maintain low temperature. NaOH solution of 10 M concentration was prepared and then added to the above solution drop wise until the pH becomes 10. Washing of the sample was done several times using a centrifuge. Methanol and distilled water were used for removing Cl^- ions and excess NaOH and SDS. The sample was dried using vacuum oven at 100 °C for 24 h and calcined in a furnace at 400 °C for 3 h. Finally, the sample was grinded using agate mortar to get the NiO nanoparticles.

Synthesis of SnO_2/NiO nanocomposite. Firstly, 50 ml isopropyl alcohol and 50 ml distilled water were mixed and then 20 g SDS was dissolved in the solution. Then stannous chloride dihydrate ($SnCl_2.2H_2O$) and nickel chloride hexahydrate ($NiCl_2{\cdot}6H_2O$) in the weight ratio of 1:1, 1:3, 1:5 and 1:7 for SN1, SN3, SN5 and SN7 samples respectively were added to the prepared solution and mixed with the help of sonicator in ice bath to maintain low temperature. NaOH solution of 10 M concentration was prepared and then added to the above solution dropwise until the pH becomes 10. Then washing of the sample was done several times by centrifuge. Methanol and distilled water were used for removing Cl^- ions and excess NaOH and SDS. The sample was dried using vacuum oven at 100 °C for 24 h and calcined in a furnace at 400 °C for 3 h. Finally, the sample was grinded using agate mortar to get the SnO_2/NiO nanocomposite.

Materials characterization. XRD patterns were collected by Rigaku X-ray diffractometer using radiations of wavelength $\lambda = 1.5406$ Å over the angular range of 20° to 80° for SnO_2/NiO nanocomposite. Intensity of the diffracted radiations was recorded as a function of 2θ. The scanning electron microscopy (SEM) was performed by JEOL JSM-6510LV scanning electron microscope. The morphology of SN1, SN3, SN5 and SN7 nanocomposite was examined by transmission electron microscopy (TEM) (JEOL JSM-2100A). PerkinElmer FTIR spectrophotometer was used to perform the Fourier Transform Infrared Spectroscopy measurements in the wave number ranging from 400 to 4,000 cm^{-1}. A PerkinElmer lambda UV–Vis absorption spectrophotometer was used for absorption studies in spectral range of 200–800 nm.

Electrochemical measurements. For electrode preparation of 80 wt% SnO_2/NiO nanocomposite, 10 wt% polyvinylidene fluoride (PVDF) and 10 wt% activated carbon were mixed in n-methyl-2-pyrrolidone (NMP) as the mixing media. The mixture was then grinded using mortar to make fine slurry and then it was

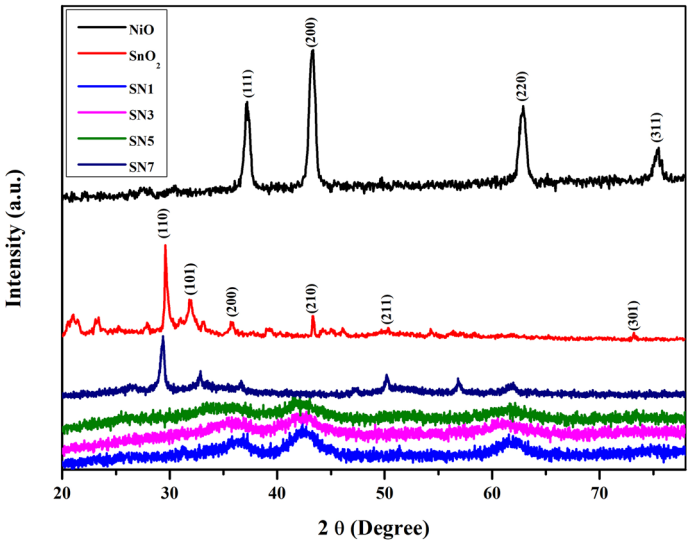

Figure 1. XRD patterns of SnO_2, NiO, SN1, SN3, SN5 and SN7.

coated on the tip of a glassy carbon electrode. Electrochemical measurements such as cyclic voltammetry, Galvanostatic charge–discharge (GCD) were performed at room temperature with the help of Metrohm Autolab PGSTAT204N that has three electrode configuration in 2 M KOH electrolyte solution[12]. The glassy electrode was used as working electrode, platinum wire as counter electrode and for reference electrode Ag/AgCl/3.0 M KCl was used.

Galvanostatically charge–discharge was performed at current density of 2.5 and 5 A/g in a potential range of − 1 to + 1 V. CV was carried out at various scan rates in the range from 5 to 100 mV/s. Electrochemical Impedance Spectra (EIS) analyses were performed using frequency range between 0 Hz to 50 kHz and a perturbation voltage of 10 mV/s was used.

Results and discussion

The crystal structures of SnO_2, NiO, SN1, SN3, SN5 and SN7 nanocomposite were characterized by XRD as shown in Fig. 1. The diffraction peaks of SnO_2/NiO nanocomposites were found to be at diffraction angle $2\theta = 29.4°$, 32.89°, 36.7°, 42.35°, 50.2°, 56.85° and 61.68° which are assigned to (110), (101), (111), (200), (211), (002) and (310) crystal planes of the samples, respectively. Using Scherrer's formula, the average particle size was calculated. The approximate crystallite sizes in the powder samples were estimated to be 48.2, 22.63, 19.24, 13.17, 4.89 and 4.53 nm for SnO_2, NiO, SN1, SN3, SN5 and SN7, respectively. Two-phase crystal structure has been clearly identified in the XRD diffraction pattern. In the XRD pattern, broad peaks having low intensity describe the tetragonal phase of SnO_2 and sharp peaks with high intensity describe the cubic phase of NiO[42,43]. On increasing the ratio of NiO in the composite, there is a broadening of peak at an angle ~ 42° that corresponds to NiO, this shows that the attachment of NiO nanoparticles increases on increasing the concentration of NiO in the composite.

Figure 2a–d shows the morphology of synthesized nanocomposites SN1, SN3, SN5 and SN7, respectively. The SEM image in Fig. 2 clearly shows that large number of particles are having homogeneous size. The energy dispersive spectroscopy (EDS) results are shown in Fig. 3. Elements oxygen, tin and nickel were present in the mesoporous SN1, SN3, SN5 and SN7, which confirms the presence and formation of SnO_2 and NiO structures. The EDS analysis exhibited clear peaks of Sn, Ni and O elements, and no additional peaks were observed, which means that the prepared Nano powder is devoid of impurities that arise from the starting precursors like chlorine and carbon.

The morphology of SN1, SN3, SN5 and SN7 nanocomposite was examined by the TEM. TEM images have been recorded using a high-resolution transmission electron microscope operating at 200 keV. Figure 4 shows the TEM micrographs of SnO_2 and NiO nanocomposite, in which clear spherical particles like structure is visible. Figure 4a shows the TEM image of SnO_2/NiO nanocomposites (SN1) revealing a spherical like structure (~ 20–22 nm) and NiO nanoparticles on the surface of SnO_2 nanoparticles matrix can be clearly seen. The particle size observed by TEM is in good agreement with that estimated by X-ray line broadening (~ 19 nm for SN1 sample). The NiO nanoparticles were well distributed onto SnO_2 nanoparticles and the inset shows the distribution at higher magnification. The TEM image also shows the tight contact between NiO and SnO_2 nanoparticles suggesting the strong interaction between the two substances. It is clear from Fig. 4a–d that correspond to the TEM images of SN1, SN3, SN5 and SN7 respectively, the size of nanocomposites decreased (from ~ 22 nm to ~ 5) with the increase in NiO concentration. The size reduction with the NiO concentration is in good agreement with the XRD studies. Figure 5 shows the selected area electron diffraction (SAED) pattern of SN1, SN3, SN5 and SN7, which confirms the polycrystalline nature of the nanocomposite. Multiple rings are seen in SAED spectrum, as expected from the XRD pattern.

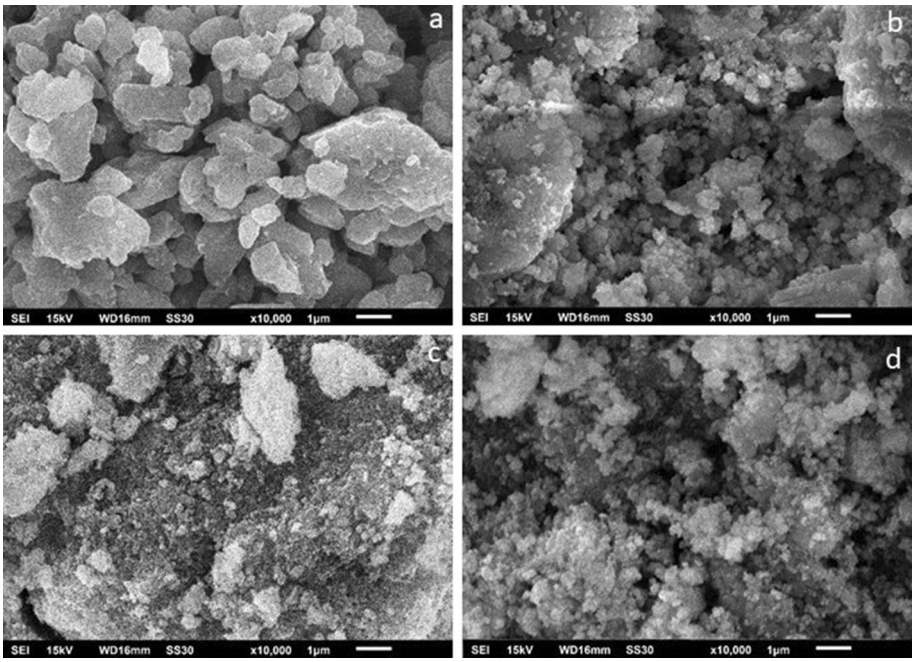

Figure 2. SEM images of (**a**) SN1, (**b**) SN3, (**c**) SN5 and (**d**) SN7.

Figure 6 shows the FTIR spectra of SnO_2, NiO, SN1, SN3, SN5 andSN7 nanocomposites. The peak at around 614–930 cm^{-1}, which refers to Sn–O stretching modes of Sn–O–Sn, appeared even after calcination at 400 °C. The band around 1,100 cm^{-1} is associated with the C=O. The band around 1,400 cm^{-1} is associated with the stretching bands of COO– group. The band around 3,390 cm^{-1} is associated with the O–H stretching. Shifting of peak was clearly shown in the graph for NiO/SnO_2 nanocomposite with the peak at 545 cm^{-1}[44,45].

UV–Vis absorption spectra of SnO_2, NiO, SN1, SN3, SN5 and SN7are shown in Fig. 5. SnO_2 and NiO nanoparticles shows characteristic peaks at 390 nm and 380 nm respectively as shown in Fig. 7. The absorption peak at 295 nm in the SnO_2/NiO confirmed the covalent attachment of SnO_2 and NiO nanoparticles.

The band gap of the samples was calculated using the following equation derived by Tauc's relation[46].

$$\alpha h\upsilon = K\left(h\upsilon - E_g\right)^n \tag{1}$$

where α is the coefficient of absorption, hυ is the incident light energy, E_g is the optical energy band gap and n is a number used to characterize the optical absorption processes. $n = 1/2$ for direct transition and $n = 2$ for indirect transition for high absorbing region, where α obeyed the above equation. By plotting $(\alpha h\upsilon)^2$ as a function of photon energy hυ (eV) and extrapolating the linear regions of this curve to $(\alpha h\upsilon)^2 = 0$ the band gap of the material was determined as shown in Fig. 8.

The value of band gaps in SnO_2, NiO, SN1, SN3, SN5 and SN7 were found to be 3.43 eV, 3.98 eV, 3.495 eV, 3.39 eV, 3.36 eV & 3.252 eV respectively. On increasing the weight percent of NiO in the composite the band gap of the nanocomposite was found to decrease, even though the particle size of the material decreases. This phenomenon shows the opposite behavior, usually the size of the particle has reverse relation with the bandgap, and size in this study was reduced, so bandgap should increase. In this case, the reason for opposite behavior is due to the increase in weight percent of NiO. This behavior is in good agreement with the results already reported by Chun-Ming et al.[46] and Azam et al.[47]. Rakhshani et al. proposed that this has been due to the direct indirect transition[48]. Many group has also suggested that the band gap narrowing effect may be due to the impurity phases that arises due to the alloying effect of parent compound[49,50].

Figure 9 shows the Galvanostatic charge/discharge curve of SnO_2, NiO, SN1, SN3, SN5 and SN7 for 1st and 10th cycle from a voltage range of − 1 V to + 1 V at a current density of 2.5 A/g. The specific capacitance is calculated over a limited potential window, hence it changes for wider or narrower potential window. Therefore, in our case the specific capacity has been calculated by multiplying the specific capacitance with width of potential window[51] as it gives consistent value and can be used for comparison with other materials.

For the calculation of specific capacitance, following formula was used[52]

$$C_s = \frac{Q}{m\Delta V} \tag{2}$$

Here C_s is the specific capacitance of the material (F/g), ΔV is the potential window used (V), m is the active material mass (g), Q is the charge stored in the full cycle. The obtained values of specific capacitance (F/g) for SnO_2, NiO, SN1, SN3, SN5 and SN7 at scan rates of 5, 10, 25, 50 and 100 mV/s are given in Table S1.

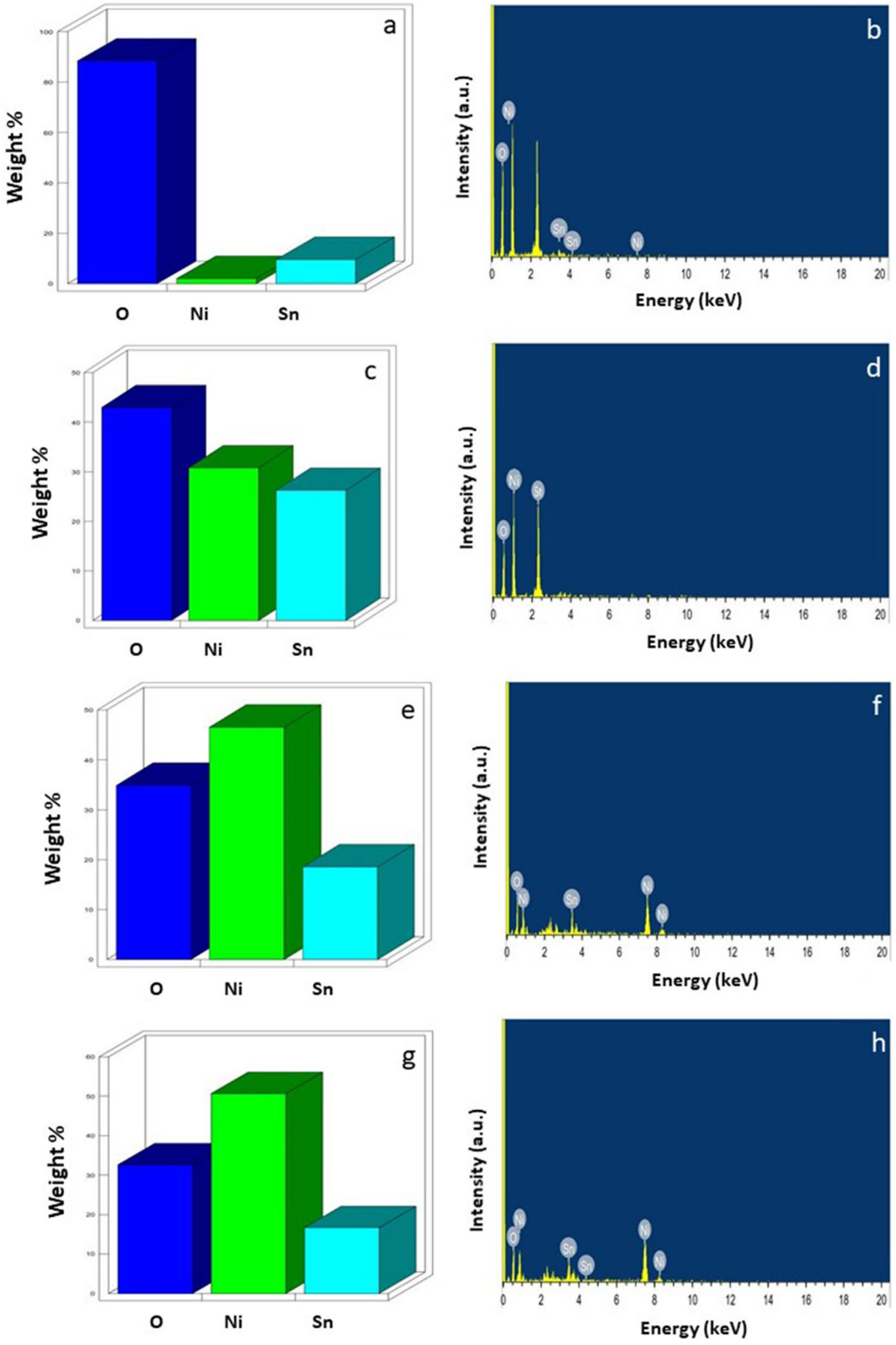

Figure 3. EDS spectra showing the composition of constituent elements Oxygen, Nickel and Tin in (**a**) and (**b**) SN1, (**c**) and (**d**) SN3, (**e**) and (**f**) SN5 and (**g**) and (**h**) SN7.

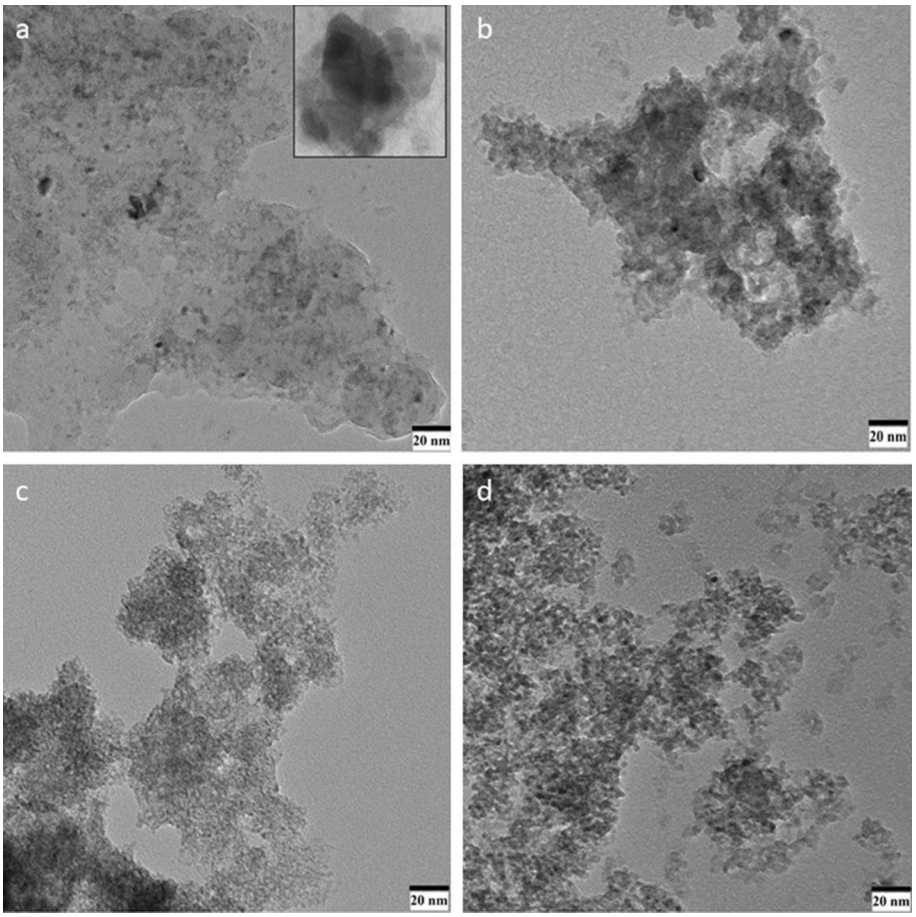

Figure 4. TEM images of (**a**) SN1, (**b**) SN3, (**c**) SN5 and (**d**) SN7.

Due to the ion exchange mechanism, the specific capacitance of the material decreases on higher scan rates[52]. It is clearly shown from the above data that the weight ratio of $NiCl_2{\cdot}6H_2O$ over $SnCl_2{\cdot}2H_2O$ have remarkable effects on the electrochemical properties of SnO_2–NiO nanocomposite. It is evident from the data that the value of C_s increases on increasing the ratio of Ni over Sn. A maximum value of C_s 464.67 F/g was observed for SN7 at scan rate of 5 mV/s. Figure 10 shows the specific capacitance values of SnO_2, NiO, SN1, SN3, SN5 and SN7 at the scan rates of 5, 10, 25, 50, and 100 mV/s for a potential window of − 1 to + 1 V. From the graph, it can be clearly seen that the value of specific capacitance is decreasing on increasing the scan rate. The maximum value of specific capacitance was obtained at a lower scan rate of 5 mV/s for SN7.

Figure S1 shows the cyclic voltammetry (CV) curves of for SnO_2, NiO, SN1, SN3, SN5 and SN7 nanocomposites at the different scan rates of 5, 10, 25, 50, and 100 mV/s in the potential window of − 1 to + 1 V. The bend shows a semi-rectangular shape, demonstrating a perfect capacitive behavior. Moreover, the linear increment of the current with an increment of scan rate demonstrates that the charge is essentially non-faradic in nature.

The charge–discharge conduct of the SnO_2, NiO, SN1, SN3, SN5 and SN7 nanocomposites electrode was inspected by Galvanostatic charge release strategy at a consistent current density of 2.5 A/g and 5 A/g in the potential range from − 1 to + 1 V. The obtained values of specific capacitance (F/g) for SnO_2, NiO, SN1, SN3, SN5 and SN7 at current rates of 2.5 A/g and 5 A/g are given in Table S2. Figure S2(a–f) demonstrates a typical Galvanostatic charge–discharge curve of SnO_2, NiO, SN1, SN3, SN5 and SN7 nanocomposites electrode. Figure 11a, b shows the Galvanostatic charge–discharge curves of different samples at 2.5 A/g and 5 A/g (V–t curve) respectively. It is clear that the whole curve is linear and symmetrical for all samples, which demonstrates that the electrode has perfect capacitive quality and amazing electrochemical reversibility.

For the calculation of specific capacitance in case of charge–discharge curve the following formula was used

$$C_s = \frac{i\Delta t}{m\Delta V} \tag{3}$$

where i is the discharging current, Δt is the discharging time and m is the loading mass of the sample on current collector. Table S3 shows the different loading mass of the sample taken on the current collector.

From the above data, it has been observed that the specific capacitance of SN7 has the maximum value of 253.94 F/g at the current density of 2.5 A/g (see Table S2) that supports the result observed from CV that is specific capacitance of the SnO_2–NiO increases on increasing the mass ratio of $NiCl_2{\cdot}6H_2O$ over $SnCl_2{\cdot}2H_2O$.

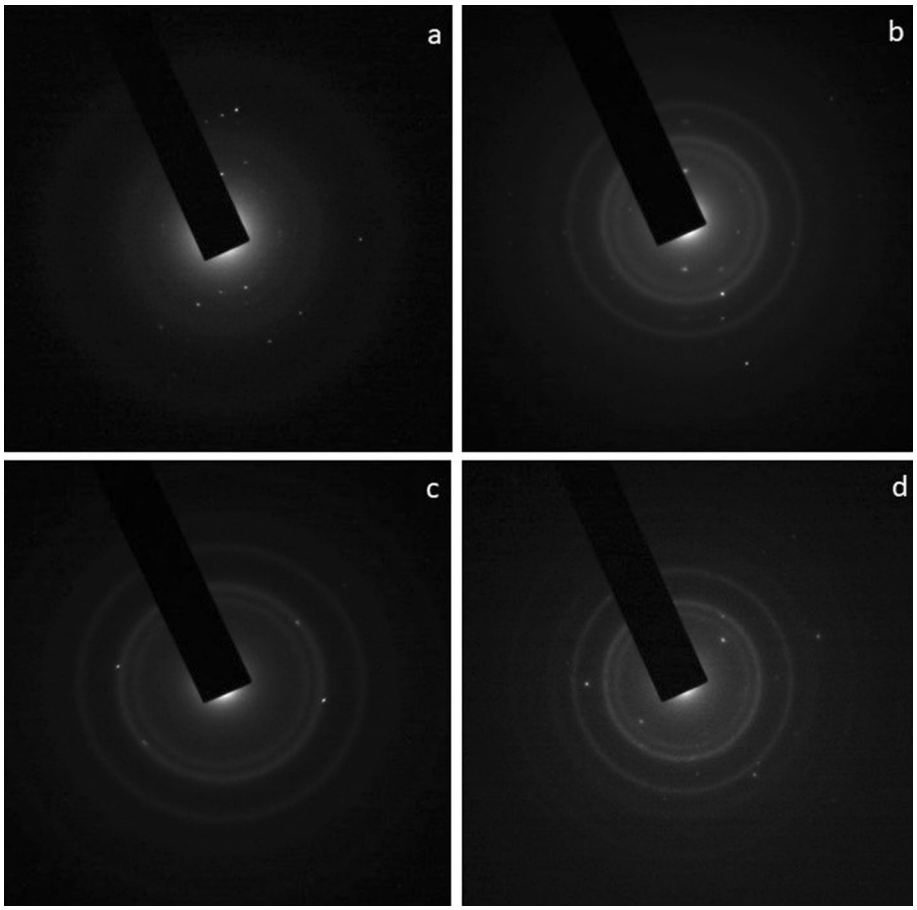

Figure 5. SAED patterns of (**a**) SN1, (**b**) SN3, (**c**) SN5 and (**d**) SN7.

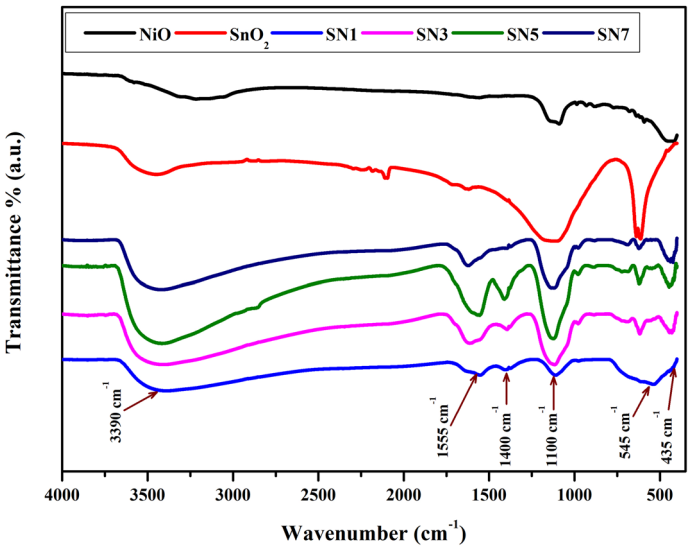

Figure 6. FT-IR spectra of SnO_2, NiO, SN1, SN3, SN5 and SN7.

Figure 12 represents the electrochemical impedance spectra (EIS) for SnO_2, NiO, SN1, SN3, SN5 and SN7 nanocomposite in the form of Nyquist plots that were recorded using complex impedance spectroscopy technique. EIS analysis was performed by applying a perturbation voltage of 10 mV/s in a frequency range between 0 Hz and 50 kHz. The impedance spectroscopy helps us to distinguish between the grains and grain boundaries contribution as both have different relaxation time. In general, the grain boundaries (poorly conducting) are

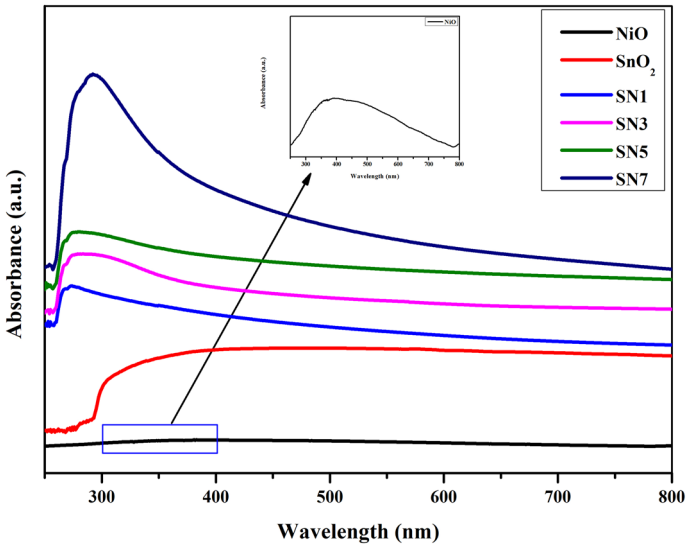

Figure 7. UV–Vis absorption spectra of SnO_2, NiO, SN1, SN3, SN5 and SN7 and NiO absorbance in inset.

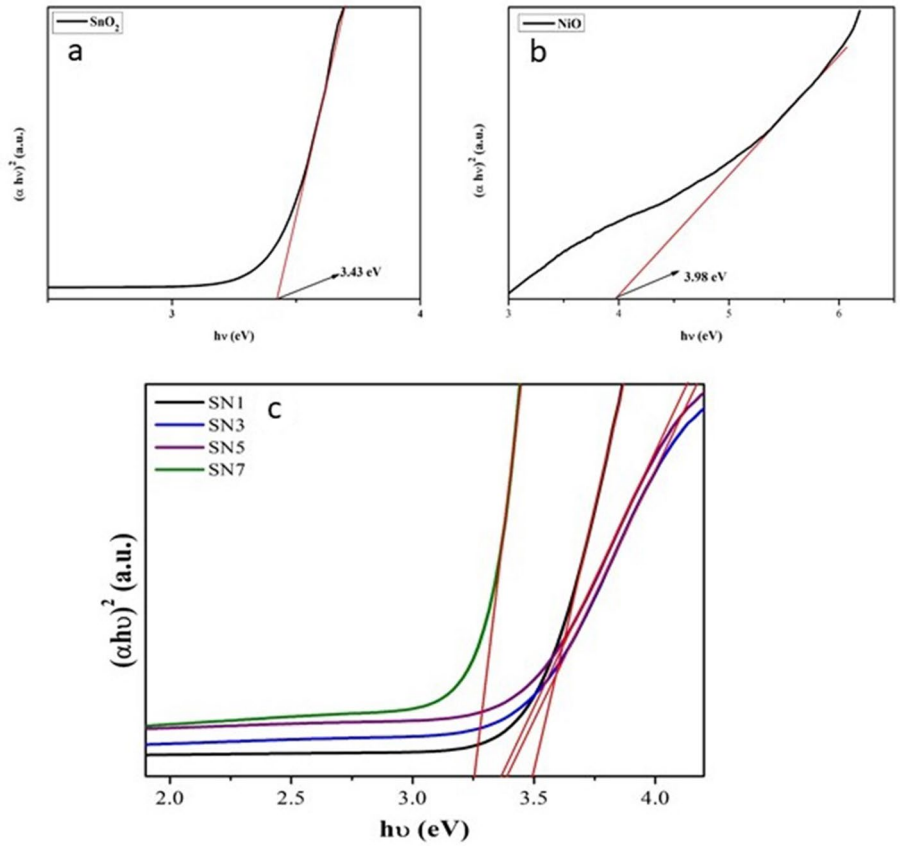

Figure 8. Energy band gap plot of (**a**) SnO_2, (**b**) NiO, (**c**) SN1, SN3, SN5 and SN7.

more active at lower frequencies whereas the conducting grains are dominant if the frequency of applied field increases[53]. The Nyquist plot shows the presence of a single circular arc for all samples, which reveals the conduction of grain boundaries only. In addition, it can also be observed that impedance increases with increasing weight percent of NiO resulting in decrement of conductivity that corresponds to the increase in specific capacitance.

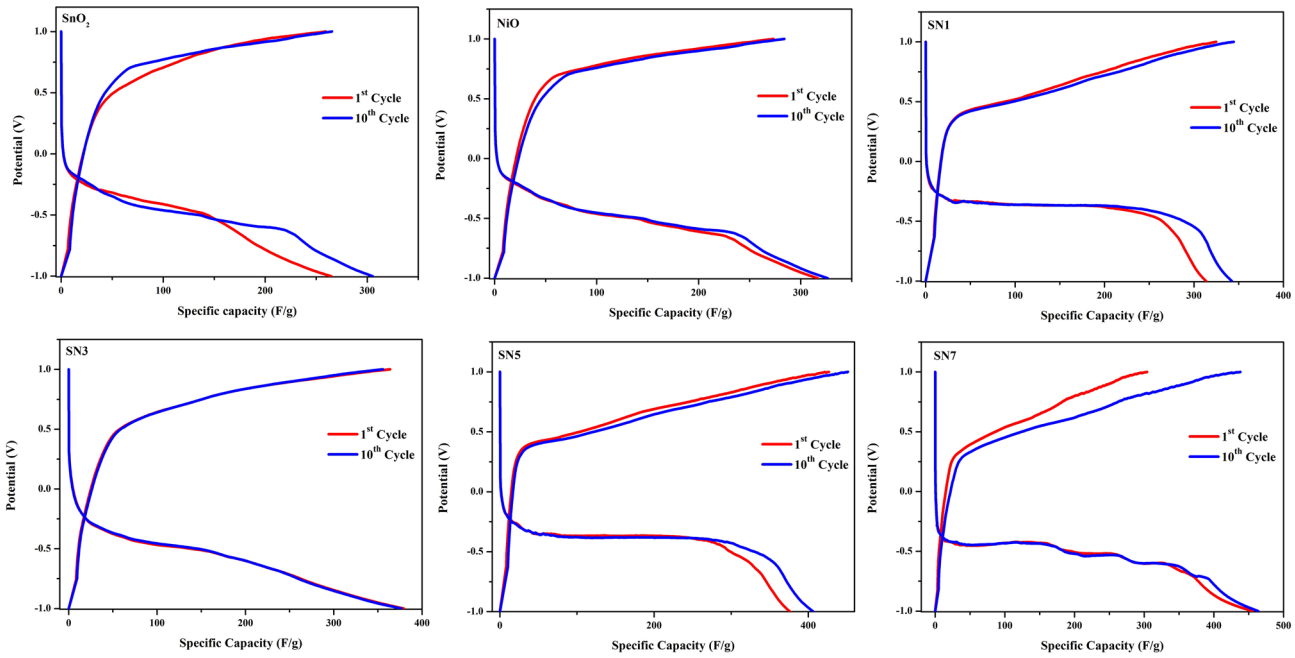

Figure 9. Galvanostatic charge/discharge curve of SnO_2, NiO, SN1, SN3, SN5 and SN7 for 1st and 10th cycle at a current density of 2.5 A/g.

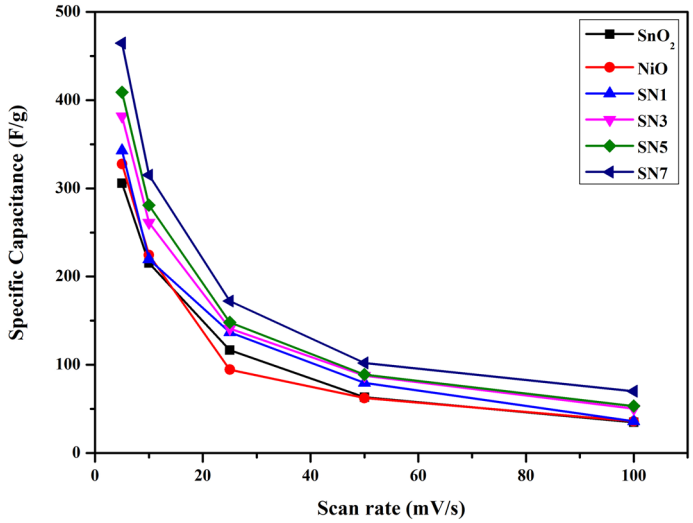

Figure 10. Specific capacitance of SnO_2, NiO, SN1, SN3, SN5 and SN7 at different scan rates.

Long term cycling test has been done to evaluate the cycling stability of the as synthesized sample SN7. Figure 13a shows the cyclic performance at a current density of 1 A/g for SN7 over 1,000 cycles. The value of specific capacitance of ~ 400.16 F/g and a capacitance retention of 87.24% was found to be retained even after 1,000 cycles, which shows a good charge–discharge behavior[54,55]. Zhang et al.[54] reported that three-dimensional self-assemble polypyrrole@$MnCo_2O_4$ nanoarchitectures on graphite foam shows capacitance retention of 85.3% after 1,000 cycles, in addition there is no loss in capacitance even after 10,000 cycles with capacitance retention of 85.5%. In another report, Zhu et al.[55] showed that a three-dimensional (3D) free-standing polypyrrole@$NiCo_2S_4$/GF electrode could deliver a high rate performance of 84.4% retention after 1,000 cycles. It is obvious that the material used in our research is different from that of the above mentioned references; instead, the cyclic stability of our supercapacitor electrode material (SnO_2/NiO nanocomposite) is comparable to the reported results, which clearly indicates that the material used in our research has great potential application for supercapacitor. Figure 13b shows the CV curves before and after cycling test at a scan rate of 20 mV/s, both CV curves are similar with two-redox peaks. However, after cycling, the potential difference is smaller between the oxidation/reduction peaks.

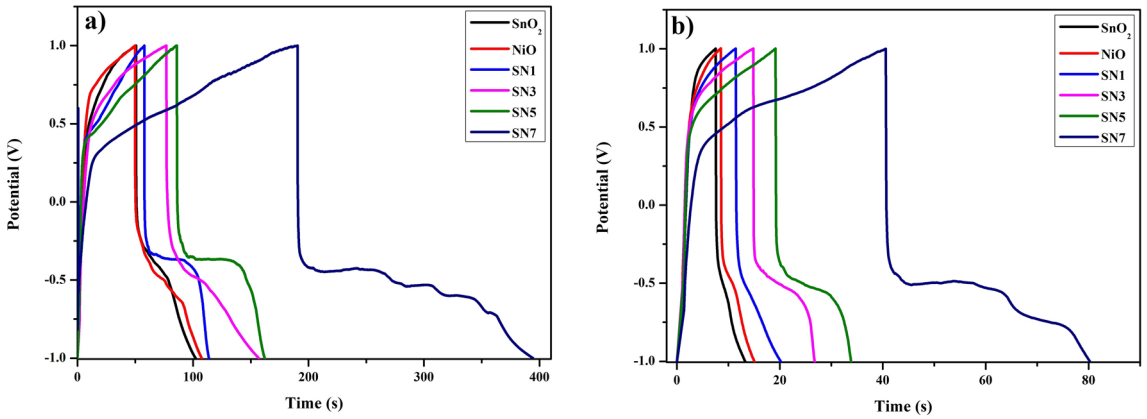

Figure 11. Galvanostatic charge–discharge curves of different samples at (**a**) 2.5 A/g and (**b**) 5 A/g (V–t curve).

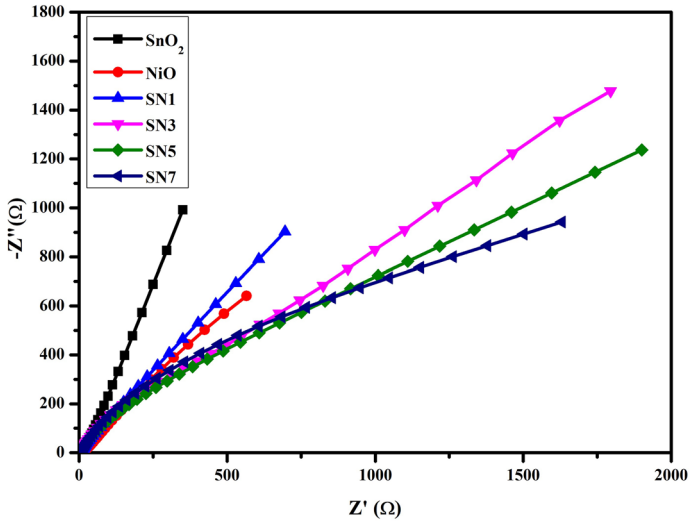

Figure 12. Electrochemical impedance spectra for SnO_2, NiO, SN1, SN3, SN5 and SN7 from 0 Hz to 50 kHz in the form of Nyquist plots.

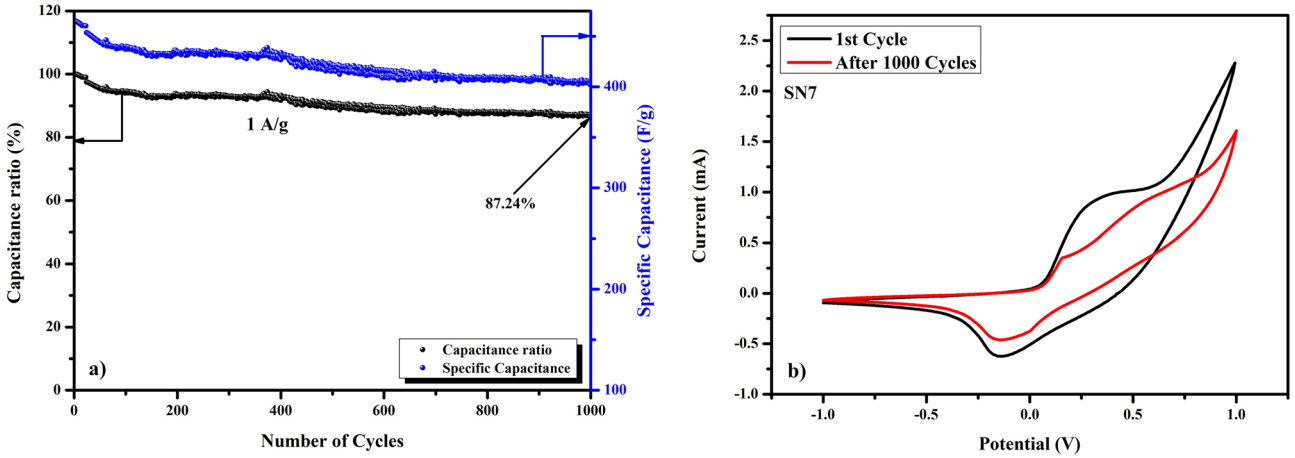

Figure 13. (**a**) Long term cycling stability and (**b**) CV curves before and after cycling.

Sample	Specific capacitance	Reference
SnO_2	122 F/g at 5 mV/s	[12]
CS@NiO	270.4 F/g at 0.5 A/g	[40]
Hollow SnO_2 microspheres	178.86 F/g at 1 mV/s	[31]
Mesoporous NiO nanowires	348 F/g at 10 mV/s	[56]
Mesoporous SnO_2@NiO	464.67 F/g at 5 mV/s	Present work

Table 1. Comparison with previous work.

Conclusion

In summary, a modified sol gel method has been developed for the synthesis of mesoporous SnO_2–NiO nanocomposites and the nanocomposites so prepared were employed as a supercapacitor electrode. XRD results confirmed that the phase purity and nanocrystalline formation of SnO_2–NiO nanocomposites and size of the particles depends on the concentration of NiO. These parameters were found to decrease on increasing the concentration of NiO in the samples, which resulted in an increase of specific capacitance. UV–Vis spectra showed a decrease in band gap of the composites on increasing the concentration of NiO that is lowest in case of SN7. SEM images showed that these nanocomposites appear to be spherical in shape and have mesoporous structure. The mesoporous structure of the synthesized material provides a high active surface for electron transfer and results in high specific capacitance. The electrochemical tests showed that the prepared SnO_2–NiO nanocomposite electrode exhibited an ideal capacitive behavior with a maximum specific capacitance of 464.67 F/g at a scan rate of 5 mV/s. Table 1 shows the comparison of specific capacitance with previously synthesized nanomaterials. A good electrochemical response was observed in terms of specific capacity in Galvanostatic charge–discharge, rate capability, cyclic stability and Coulombic efficiency. This excellent performance is due to the mesoporous structure of the prepared composite. These results demonstrate that the prepared SnO_2–NiO nanocomposites are suitable candidates and more attractive electrode material for the commercial supercapacitors applications.

Received: 30 July 2019; Accepted: 23 April 2020
Published online: 03 July 2020

References

1. Singh, A. & Chandra, A. Graphene and graphite oxide based composites for application in energy systems. *Phys. status solidi b* **1487**, 1483–1487 (2013).
2. Luo, X., Wang, J., Dooner, M. & Clarke, J. Overview of current development in electrical energy storage technologies and the application potential in power system operation. *Appl. Energy* **137**, 511–536 (2015).
3. Aricò, A. S. *et al.* Nanostructured materials for advanced energy conversion and storage devices. *Nat. Mater.* **4**, 366–377 (2005).
4. Chandra, A., Roberts, A. J., Lam, E., Yee, H. & Slade, R. C. T. Nanostructured oxides for energy storage applications in batteries and supercapacitors*. *Pure Appl. Chem.* **81**, 1489–1498 (2009).
5. Yu, Z., Tetard, L., Zhai, L. & Thomas, J. Supercapacitor electrode materials: nanostructures from 0 to 3 dimensions. *Energy Environ. Sci.* **8**, 702–730 (2015).
6. Yan, J., Wang, Q., Wei, T. & Fan, Z. Recent advances in design and fabrication of electrochemical supercapacitors with high energy densities. *Adv. Energy Mater.* **4**, 1300816 (2014).
7. Xiong, S., Yuan, C., Zhang, X. & Xi, B. Controllable synthesis of mesoporous Co_3O_4 nanostructures with tunable morphology for application in supercapacitors. *Chem. A Eur. J.* **15**, 5320–5326 (2009).
8. Augustyn, V. *et al.* Pseudocapacitive oxide materials for high-rate electrochemical energy storage. *Energy Environ. Sci.* **7**, 1597–1614 (2015).
9. Xie, Y. *et al.* Mixed transition-metal oxides: Design, synthesis, and energy-related applications . *Angew. Chem.* **53**, 1488–1504 (2014).
10. Chandra, A., Roberts, A. J. & Slade, R. C. T. Nanostructured vanadium oxide based systems: Their applications in supercapacitors. *Int. J. Nanotechnol.* **7**, 861–869 (2010).
11. Sk, M., Yue, C. Y., Ghosh, K. & Jena, R. K. Review on advances in porous nanostructured nickel oxides and their composite electrodes for high-performance supercapacitors. *J. Power Sources* **308**, 121–140 (2016).
12. Manikandan, K., Dhanuskodi, S., Maheswari, N. & Muralidharan, G. SnO_2 nanoparticles for supercapacitor application. *AIP Conf. Proc.* **1731**, 50048 (2016).
13. Xu, S., Zhang, Y., Guo, J. & Wang, C. Fe_3O_4@coordination polymer microspheres with self-supported polyoxometalates in shells exhibiting high-performance supercapacitive energy storage†. *Chem. Commun. RSC* **49**, 2427–2429 (2013).
14. Liu, M. & Sun, J. In situ growth of monodisperse Fe_3O_4 nanoparticles on graphene as flexible paper for supercapacitor†. *J. Mater. Chem. A Mater. Energy Sustain. R. Soc. Chem.* **2**, 12068–12074 (2014).
15. Sun, H. *et al.* Solvothermal synthesis of tunable electroactive magnetite nanorods by controlling the side reaction. *J. Phys. Chem.* **116**, 5476–5481 (2012).
16. Xia, H. *et al.* Facile synthesis of hematite quantum-dot/functionalized graphene-sheet composites as advanced anode materials for asymmetric supercapacitors. *Adv. Funct. Mater.* **25**, 3554 (2014).
17. Sun, S. *et al.* Identifying pseudocapacitance of Fe_2O_3 in an ionic liquid and its application in asymmetric supercapacitors. *J. Mater. Chem. A Mater. Energy Sustain.* **2**, 14550–14556 (2014).
18. Lee, K. K., Chin, W. S. & Sow, C. H. Cobalt-based compounds and composites as electrode materials for high-performance electrochemical capacitors†. *J. Mater. Chem. A Mater. Energy Sustain.* **2**, 17212–17248 (2014).
19. Zhou, Z. *et al.* Amorphous RuO_2 coated on carbon spheres as excellent electrode materials for supercapacitors. *RSC Adv.* **2**, 6927–6932 (2014).
20. Park, J. H., Ko, M. & Park, O. O. Carbon nanotube@RuO_2 nanocomposite electrodes for supercapacitors. *J. Electrochem. Soc.* **150**, 864–867 (2010).
21. Gujar, T. P. *et al.* Spray deposited amorphous RuO_2 for an effective use in electrochemical supercapacitor. *Electrochem. Commun.* **9**, 504–510 (2007).

22. Chang, K. & Hu, C. Hydrothermal synthesis of hydrous crystalline RuO_2 nanoparticles for supercapacitors. *Electrochem. Solid-State Lett.* **7**, 466–469 (2004).
23. Ji, H. *et al.* In situ preparation of sandwich MoO_3/C hybrid nanostructures for high-rate and ultralong-life supercapacitors. *Adv. Funct. Mater.* **25**, 4378 (2015).
24. Lu, T. *et al.* Microwave-assisted synthesis of graphene–ZnO nanocomposite for electrochemical supercapacitors. *J. Alloys Compd.* **509**, 5488–5492 (2011).
25. Zhang, Z. *et al.* One-pot electrodeposition synthesis of ZnO/graphene composite and its use as binder-free electrode for supercapacitor. *Ceram. Int.* **41**, 4374–4380 (2014).
26. Xue, C., Lv, Y., Zhang, F., Limin, Wu. & Zhao, D. Copper oxide activation of soft-templated mesoporous carbons and their electrochemical properties for capacitors †. *J. Mater. Chem.* **22**, 1547–1555 (2012).
27. Deng, M. *et al.* Facile electrochemical synthesis of 3D nano-architectured CuO electrodes for high-performance supercapacitors†. *J. Mater. Chem. A Mater. Energy Sustain.* **2**, 12857–12865 (2014).
28. Jo, C. *et al.* Block-copolymer-assisted one-pot synthesis of ordered mesoporous WO_{3-x}/carbon nanocomposites as high-rate-performance electrodes for pseudocapacitors. *Adv. Funct. Mater.* **23**, 2682 (2013).
29. Zhao, Q., Ma, L., Zhang, Q., Wang, C. & Xu, X. SnO_2-based nanomaterials: synthesis and application in lithium-ion batteries and supercapacitors. *J. Nanomater.* **2015**, 1–15 (2015).
30. Aziz, M., Abbas, S. S., Rosemaria, W. & Baharom, W. Size-controlled synthesis of SnO_2 nanoparticles by sol–gel method. *Mater. Lett.* **91**, 31–34 (2013).
31. Yang, Y., Ren, S., Ma, S., Hao, C. & Ji, M. Electrochimica acta hollow tin dioxide microspheres with multilayered nanocrystalline shells for pseudocapacitor. *Electrochim. Acta* **155**, 437–446 (2015).
32. Zhou, F., Liu, Q., Gu, J., Zhang, W. & Zhang, D. A facile low-temperature synthesis of highly distributed and size-tunable cobalt oxide nanoparticles anchored on activated carbon for supercapacitors. *J. Power Sources* **273**, 945–953 (2015).
33. Augustyn, V., Simon, P. & Dunn, B. Environmental science pseudocapacitive oxide materials for high-rate electrochemical energy storage. *Energy Environ. Sci.* **7**, 1597–1614 (2014).
34. Feng, L., Zhu, Y., Ding, H. & Ni, C. Recent progress in nickel based materials for high performance pseudocapacitor electrodes. *J. Power Sources* **267**, 430–444 (2014).
35. Wang, L. *et al.* Reduced graphene oxide/nickel cobaltite nanoflake composites for high specific capacitance supercapacitors. *Electrochim. Acta* **111**, 937–945 (2013).
36. Wang, F. *et al.* Co-doped Ni_3S_2@CNTs array anchored on graphite foam with hierarchical conductive network for high-performance supercapacitor and hydrogen evolution electrode. *Mater. Chem. A* **6**, 10490–10496 (2018).
37. Wang, F. *et al.* P-doped $NiMoO_4$ parallel arrays anchored on cobalt carbonate hydroxide with oxygen vacancies and mass transfer channels for supercapacitor and oxygen evolution. *J. Mater. Chem. A* **7**, 19589–19596 (2019).
38. Huang, M. *et al.* Facile synthesis of single-crystalline NiO nanosheet arrays on Ni foam for high-performance. *CrystEngComm* **16**, 2878–2884 (2014).
39. Ouyang, B., Zhang, Y., Zhang, Z., Fan, H. J. & Rawat, R. S. Nitrogen-plasma-activated hierarchical nickel nitride nanocorals for energy applications. *Small* **13**, 1–10 (2017).
40. Le, Q., Wang, T., Zhu, S., Zhang, J. & Zhang, Y. Facile synthesis of carbon sphere@$Ni(OH)_2$ and derivatives for high-performance supercapacitors. *Funct. Mater. Lett.* **9**, 2–6 (2016).
41. Shown, I., Ganguly, A., Chen, L. & Chen, K. Conducting polymer-based flexible supercapacitor. *Energy Sci. Eng.* **3**, 2–26 (2014).
42. Hieu, N. V. *et al.* Giant enhancement of H2S gas response by decorating n-type SnO_2 nanowires with p-type NiO nanoparticles Giant enhancement of H_2S gas response by decorating n-type SnO_2 nanowires with p-type NiO nanoparticles. *Appl. Phys. Lett.* **101**, 253106-1-253106–4 (2012).
43. Rensheng, S., Xiangping, L. I., Xiaochuan, X. I. A., Hongwei, L. & Guoguang, W. U. Comparative investigation of three types of ethanol sensor based on NiO–SnO_2 composite nanofibers. *Chin. Sci. Bull.* **57**, 2087–2093 (2012).
44. Hamzah, F. I. & Khalid, K. Better adsorption capacity of SnO_2 nanoparticles with different graphene addition Better adsorption capacity of SnO_2 nanoparticles with different graphene addition. *J. Phys.* **776**, 1–6 (2016).
45. Nedumkallel, A. S., Sabu, B. & Varghese, T. Effect of calcination temperature on structural and optical properties on nickel oxide nanoparticles. *Nanosystems* **5**, 441–449 (2014).
46. Grigorovici, R. & Vancu, A. Optical properties and electronic structure of amorphous germanium. *Phys. Stat. Solut.* **15**, 627–637 (1966).
47. Ahmed, A. S. *et al.* Band gap narrowing and fluorescence properties of nickel doped SnO_2 nanoparticles. *J. Lumin.* **131**, 1–6 (2011).
48. Rakhshani, A. E., Makdisi, Y. & Ramazaniyan, H. A. Electronic and optical properties of fluorine-doped tin oxide films. *J. Appl. Phys.* **83**, 1049–1057 (2012).
49. Search, H. *et al.* The influence of nickel dopant on the microstructure and optical properties of SnO_2 nano-powders*. *IOP Sci.* **16**, 95–99 (2007).
50. Marsillac, S., Mokrani, A., Barreau, N. & Bern, J. C. Study of low temperature elaborated tailored optical band gap b-$In_2S_{3-3x}O_{3x}$ thin films. *J. Cryst. Growth* **235**, 439–449 (2002).
51. Brousse, T. & Daniel, B. JES: Focus issue on electrochemical capacitors: Fundamentals to applications. To be or not to be pseudocapacitive?. *J. Electrochem. Soc.* **162**, 5185–5189 (2015).
52. Nagamuthu, S., Vijayakumar, S. & Muralidharan, G. Ag incorporated Mn_3O_4/AC nanocomposites based supercapacitor devices with high energy density and power density. *Dalt. Trans.* **43**, 17528–17538 (2014).
53. Hassan, M. & Glass, C. Structural and frequency dependent dielectric properties of Fe^{3+} doped ZnO nanoparticles. *Mater. Res. Bull.* **47**, 3952–3958 (2012).
54. Zhang, Y. *et al.* Construction of vertically aligned PPy nanosheets networks anchored on $MnCo_2O_4$ nanobelts for high-performance asymmetric supercapacitor. *J. Power Sources* **393**, 169–176 (2018).
55. Zhu, Y. *et al.* Xiaodong GuoPPy@$NiCo_2S_4$ nanosheets anchored on graphite foam with bicontinuous conductive network for high-areal capacitance and high-rate electrodes. *J. Alloys Compd.* **747**, 276–282 (2018).
56. Su, D., Kim, H., Kim, W. & Wang, G. Mesoporous nickel oxide nanowires: Hydrothermal synthesis, characterisation and applications for lithium-ion batteries and supercapacitors with superior performance. *Chem. A Eur. J.* **18**, 8224–8229 (2012).

Acknowledgements

Authors are thankful to Department of Science and Technology (DST), University Grant Commission (UGC), Government of India for providing financial support in the form of PURSE II and DRS II.

Author contributions

A.A. and B.V. contributed to the conception and design of the experiments, analysis of the data and writing the paper. B.V. carried out all experiments, and B.V. and A.H.A. performed electrochemical analyses. M.Z.K. contributed to the electrochemical analyses, and H.H.H. contributed to the electrochemical studies with long cycling stability. B.V. prepared figures and formatted the manuscript and, B.V., F.A., A.A. wrote the paper. A.A.,

B.V. and F.A. contributed in the interpretation of the results. A.A., M.J.S., A.A., F.A., and B.V. participated in the scientific discussion during the preparation of this manuscript. All authors reviewed the manuscript.

Competing interests
The authors declare no competing interests.

Additional information
Supplementary information is available for this paper at https://doi.org/10.1038/s41598-020-67990-8.

Correspondence and requests for materials should be addressed to A.A.

Reprints and permissions information is available at www.nature.com/reprints.

Publisher's note Springer Nature remains neutral with regard to jurisdictional claims in published maps and institutional affiliations.